scientific reports

Check for updates

OPEN

A MEMS seismometer respiratory monitor for work of breathing assessment and adventitious lung sounds detection via deep learning

Brian Sang[1]✉, Haoran Wen[2], Greg Junek[2], Wendy Neveu[3], Lorenzo Di Francesco[3], Justin Romberg[1] & Farrokh Ayazi[1]

Physicians evaluate a patient's respiratory health during a physical examination by visual assessment of the work of breathing (WoB) to determine respiratory stability, and by detecting abnormal lung sounds via lung auscultation using a stethoscope to identify common pathological lung diseases, such as chronic obstructive pulmonary disease (COPD) and pneumonia. Since these assessment methods are subjective, a low-profile device used for an accurate and quantitative monitoring approach could provide valuable preemptive insights into respiratory health, proving to be clinically beneficial. To achieve this goal, we have developed a miniature patch consisting of a sensitive wideband multi-axis seismometer that can be placed on the anatomical areas of a patient's lungs to enable an effective quantification of a patient's WoB and lung sounds. When used on a patch, the seismometer captures chest wall vibrations due to respiratory muscle effort, known as high-frequency mechanomyogram (MMG), during tidal breathing as well as seismic pulmonary-induced vibrations (PIVs) during deep breathing due to normal and/or adventitious lung sounds like crackles, while simultaneously recording respiration rate and phase. A system comprised of multiple patches was evaluated on 124 patients in the hospital setting and shown to accurately assess and quantify a patent's physical signs of WoB by measuring the average respiratory effort extracted from high-frequency MMG signals, demonstrating statistical significance of this method in comparison to clinical bedside observation of WoB and respiration rate. A data fusion deep learning model was developed which combined the inputs of PIVs lung sounds and the corresponding respiration phase to detect crackle, wheeze and normal breath sound features. The model exhibited high accuracy, sensitivity, specificity, precision and F1 score of 93%, 93%, 97%, 93% and 93% respectively, with area under the curve (AUC) of precision recall (PR) of 0.97 on the test set. Additionally, the PIVs with corresponding respiration phase captured from each auscultation point generated an acoustic map of the patient's lung, which correlated with traditional lung radiographic findings.

Common respiratory diseases, such as chronic obstructive pulmonary disease (COPD) and pneumonia, can lead to respiratory failure and are characterized by a wide range of symptoms and signs, including increased respiration rate, increased physical signs of work of breathing (WoB), and the presence of respiratory crackles and wheezes[1,2]. Respiratory diseases are highly prevalent, with pneumonia affecting approximately 450 million people annually, and COPD impacting about 10% of adults worldwide[3,4]. Severe COPD exacerbations can result in respiratory failure, a life-threatening condition caused by inadequate oxygen and carbon dioxide exchange in the lungs[5,6]. Notably, COPD is the third leading cause of death globally, primarily due to acute or progressive respiratory failure[6,7]. Overall, respiratory failure is the most common organ failure, costing up to $27 billion annually in US hospitals (12% of all hospital costs)[7–10]. Early detection of acute or chronic respiratory diseases and respiratory failure is crucial for successful treatment and disease management as they have progressive conditions[11,12]. Conventional radiographic instruments, while effective in detecting anatomical lung abnormalities, are bulky, expensive and time-consuming, making them unsuitable for continuous monitoring of patients[14]. Traditional vital sign measurements (respiration rate, oximetry, heart rate, etc.) are also not reliable for detecting respiratory disease and distress[13]. As a result, respiratory diseases including respiratory failure, are often underdiagnosed, undertreated, or inadequately controlled, contributing to higher hospital readmission and patient mortality[14].

[1]Georgia Institute of Technology, Atlanta, GA 30308, USA. [2]StethX Inc., Atlanta, GA 30308, USA. [3]Department of Medicine, Emory University School of Medicine, Atlanta, GA 30303, USA. ✉email: bsang3@gatech.edu

For instance, delayed treatment of hospital-acquired pneumonia, which can be indicated by tachypnea (shallow rapid breathing demonstrating high WoB) and new crackles on examination, has shown to worsen outcomes in stroke patients[15–17]. Similarly, delayed intubation of more than 30 min from initial respiratory failure signs increases morbidity and mortality significantly[18]. Despite 50 years of research, there is no *quantitative* method for detecting respiratory failure through WoB signs[19], nor a robust wearable system for continuous monitoring of lung sounds. This highlights the urgent need for a non-invasive wearable diagnostic system to assess and monitor a patient's respiratory health by simultaneously detecting changes in WoB and identifying abnormalities in the airway of their lungs[20–24].

Assessment of work of breathing is a key part of identifying respiratory distress. Work of breathing (WoB) refers to the energy required for normal (tidal) breathing and is typically assessed by physicians at bedside through observation of the patient's physical respiratory effort[25–28]. WoB is also referred to as the energy needed to move one liter of gas per respiratory cycle[29]. Both views refer to the energy needed to overcome the elastic and flow-resistive forces of the lung or chest[30], with physical signs of WoB relating to the amount of energy needed by the respiratory muscles to produce adequate ventilation for the body. These respiratory signs include the use of accessory respiratory muscles (scalene, sternocleidomastoid, intercostal, and abdominal) and respiration rate during tidal breathing, are key indicators of underlying pathology and serve as the most predictive indicator for respiratory failure at bedside[25,27,28,31–33]. Specifically, increased use of these muscles along with increased respiration rate (> 20 breaths/minute in adults over 18 years old) indicate breathing difficulty and respiratory deterioration. Severe cases may also show paradoxical breathing (abdominal wall abruptly moves inward during inhalation and outward during exhalation, opposite to normal breathing movement)[26,27], which can indicate increased respiratory failure and the need for mechanical ventilation[34].

Simultaneous measurement of muscle activity and respiration patterns presents a significant bottleneck for quantifying WoB[19]. Traditionally, muscle activity can be detected by measuring the electrical potential changes across muscle cells during muscle activation, known as electromyography (EMG), which can be captured by electrodes with activities in the 25–250 Hz range; however, EMG does not capture respiration patterns[19,35]. Alternatively, muscle activity can also be captured by measuring the mechanical vibrations observable from the skin around contracting muscles, known as mechanomyography (MMG). It has been shown that off-the-shelf accelerometers can capture low-frequency MMG in the 5–35 Hz range along with respiration patterns (0–5 Hz)[36–39], but their low resolution and limited bandwidth reduce their ability to measure chest wall vibrations with high fidelity at higher frequency range. Importantly, heart-sound-induced vibrations in the range of 5–80 Hz[40] interfere with low-frequency MMG, reducing its effectiveness in quantifying accessory respiratory muscle movements.

To address this gap, we present a lightweight, rigid, wideband seismometer patch with digital output (Fig. 1a) that detects WoB by capturing distinct high-frequency vibrations from accessory muscle activity during tidal breathing, along with low-frequency breathing patterns. This low-noise hermetically-sealed seismometer patch features out-of-plane seismometer (OPS) and in-plane seismometer (IPS) chips with digital output, enabling the distinct capture of perpendicular and tangential movements of the accessory muscle, respectively, within the 'high-frequency' range of 80–200 Hz. These movements are captured with constant gain and high fidelity, comparable to EMG frequency range, while not being interfered with potential adventitious lung sound frequencies. Detailed seismometer specifications showcasing micro-gravity acceleration with constant gain in the DC-10 kHz bandwidth of both out-of-plane and in-plane are shown in the Supplements and Supplementary Fig. 1.

The seismometer patch has large enough bandwidth and signal-to-noise ratio to also capture weak mechano-acoustic vibrations from lung sounds during deep breathing, known as pulmonary-induced vibrations (PIVs)[41–43]. Robust against ambient sounds[40,42–47], the seismometer effectively captures adventitious lung sounds, such as crackles and wheezing during a patient's deep breaths[25,43,46]. Crackles, either coarse or fine, are prevalent indicators of respiratory disease with distinct respiration patterns and acoustic signatures that often aid in the clinical diagnosis process[48]. For example, early inspiratory coarse crackles in the basal lung regions, detected by a physician with a stethoscope, strongly correlate with COPD in patients with risk factors like tobacco use[49,50]. However, crackles are faint signals and thus challenging for less experienced professionals to detect with a stethoscope[51,52]. Another important adventitious lung sound is wheezing, a high-pitched whistling sound from the lungs[48,53], which also indicates the patient's respiratory status, as shown in Supplementary Table 1[48,54–56].

Using the wideband seismometer patch, we present a non-invasive approach for monitoring a patient's respiratory status, including WoB and adventitious lung sounds detection. We quantified WoB by calculating the average respiratory effort of accessory muscles using high-frequency MMG signals of each respiratory cycle, identified via low-frequency signal peak detection during tidal breathing. To determine statistical significance between normal and increased respiratory effort, each patient's high-frequency MMG data was compared with physician's visual assessments, the clinical benchmark for a patient's increased WoB[26,27,31,36–38,57–59]. Notably, paradoxical abdominal breathing patterns were also captured by the seismometer patch. Additionally, we developed the first of its kind early data fusion 2D convolutional neural network (CNN) that integrates lung sounds and respiration cycle as inputs, based on clinical correlation as shown in Supplementary Table 1[42,48], to automatically detect crackles, wheezing and normal breath sounds from PIVs during deep breathing. To the best of our knowledge, this is the first report of a microchip seismometer being used as a respiratory monitor system, including the first quantification of physical signs of WoB. With the capability to support multiple sensor heads for simultaneous data capture, this system can also effectively cover accessory muscles and various lobar segments of the lung, pinpointing the sources of abnormalities. This framework can enable the creation of an acoustic map of the lung, which can be correlated with radiographic instruments like X-Rays and Computed Tomography (CT) scans of the lung[60–63].

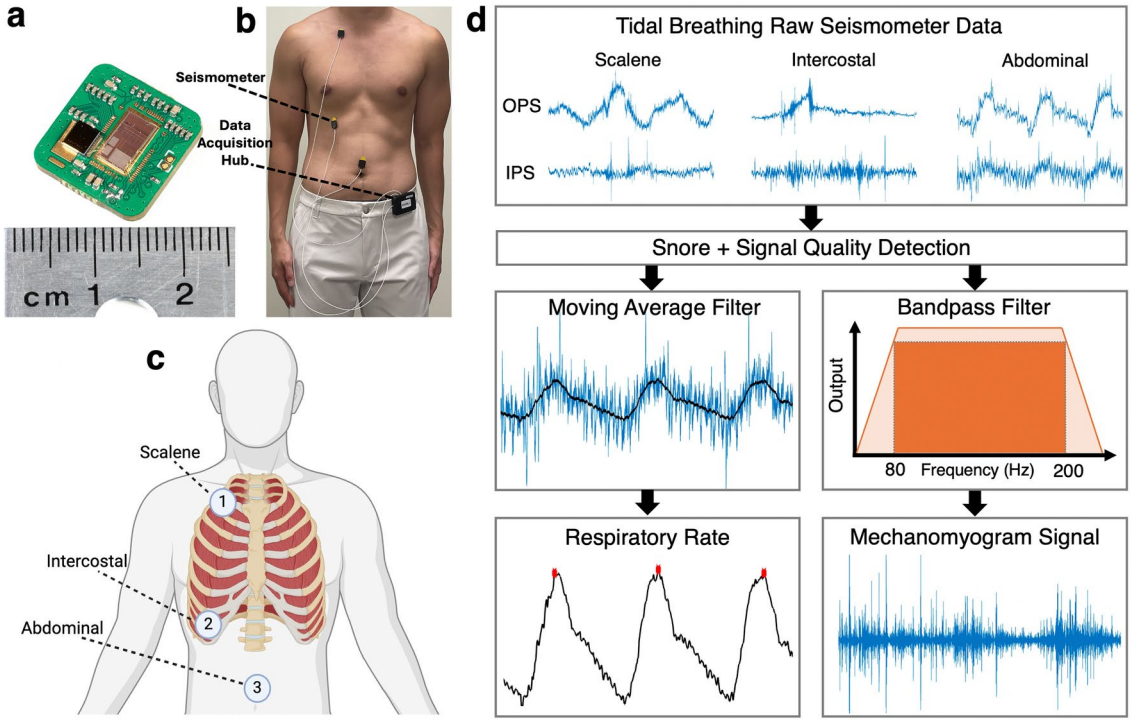

Fig. 1. Seismometer patch with nanogaps for work of breathing detection. (**a**) The seismometer, which encompasses both the MEMS die and CMOS ASIC. (**b**) The seismometer patches were taped on the body with on all corresponding work of breathing locations; the sensors are connected to a data acquisition hub similar to a Holter monitor. (**c**) For WoB quantification, the seismometer patches were placed on each of the three WoB locations on the anterior right chest walls. (**d**) The raw tidal breathing data from the scalene, intercostal and abdominal regions were collected from both the out-of-plane seismometer (OPS) and in-plane seismometer (IPS) chips. The data first undergoes a snore and signal quality detection to exclude non-tidal breathing data. The cleaned raw data is then filtered with a moving average filter to capture the respiration pattern, followed by peak detection (marked by red stars) to determine respiration rate. The cleaned raw data is also bandpass filtered from 80 to 200 Hz to isolate the high-frequency mechanomyogram signal. During data collection, physicians simultaneously observe for respiration rate and respiratory effort as a clinical benchmark for comparison.

Methods

Participants

We conducted a study using the seismometer patch involving 124 patients across diverse demographics and a wide variety of clinical characteristics examined in either the hospital setting or outpatient asthma clinic. Work of breathing measurement during tidal breathing were taken from 28 patients and lung sound recordings during deep breathing were taken from 96 other patients, both at Grady Memorial Hospital in Atlanta, Georgia, USA. The patients had varying demographics such as age, height, weight and BMI as shown in Supplementary Table 2, 4 and 7. All the human subjects participated voluntarily with written informed consent. Patients were tested in the hospital and the outpatient pulmonary asthma clinic. In the hospital (emergency room and general hospital beds), patients were chosen through blind referrals given to the physician for patients with a variety of respiratory disorders likely to exhibit increased WoB and adventitious lung sounds. In the outpatient asthma clinic, patient selection was guided by a diverse range of severity of asthma and lung sounds. The protocol was approved by Emory University and Georgia Institute of Technology Institutional Review Board (IRB #00105563). The process of data collection from patients was supervised by experienced and authorized physicians. All experiments were performed in accordance with relevant guidelines and regulations.

Study protocol

For the 28 patients undergoing WoB assessment, the seismometer patches were placed on the patient's chest walls secured via 3 M 2764 medical tape on three WoB sites or each of the nine auscultation sites, as shown in Figs. 1c and 3a, respectively. The seismometer sensor board was connected via wire to a data acquisition hub unit as shown in Fig. 1b. After data collection, the diagnosis of the patient's clinical disease was provided by the physician after clinical evaluation and/or chart review.

For the WoB study protocol, each patient was asked to either sit or lie down, based on their comfort, and asked to breathe normally. The seismometer patches, consisting of OPS and IPS, were placed on each of the patient's accessory muscle groups (scalene, intercostal and abdominal), placed on their right side to reduce heart sound artifacts due to the mechanical signal of the heart, for 30 s intervals, as shown in Fig. 1c. Physician

assessment of WoB was conducted independently by a dedicated research physician who is an internal medicine trained physician with 28 years in clinical practice experience as a standard operating procedure for measuring physical examination for each patient's respiratory status which included evaluating for the following: the respiratory rate as well as objective evidence of increased work of breathing (presence of intercostal muscle and/or scalene muscle use and evaluating for abdominal muscle use during expiration and looking for the presence of abdominal paradox (which is an abdomen that is going inward on inspiration which is a severe finding of acute respiratory distress indicating excessive air trapping and hyperinflated diaphragms unable to move down to cause inspiration so the abdomen moves inward and the chest up and outward by the patient's heightened accessory muscle activation). After collecting data from 28 patients, the output was analyzed during patients' tidal breathing[64] where 9 patients exhibited increased scalene respiratory effort, 9 showed increased intercostal effort, and 8 had increased abdominal effort. Some patients had increased effort in multiple accessory muscle groups with details of each patient's work of breathing status in Supplementary Table 3. Overall patient demographics and distribution of normal and increased respiratory effort are shown in Supplementary Table 4 and 5, respectively.

For the lung study protocol, each of the 96 patients was asked to either sit or lie down and to take continuous deep breaths first with a stethoscope for a traditional lung auscultation exam and then the seismometer patches were placed for 30 s intervals for each of the nine auscultation areas, as shown in Fig. 3a, to cover the five major lobes of the human lungs (right superior, right middle, right inferior, left superior and left inferior lobes) for adventitious lung abnormalities. The diagnosis of the patient's clinical disease was provided by the physician after their clinical evaluation and/or chart review. After collecting lung auscultation data from 96 patients from the auscultation sites for 30 s each, a different experienced physician, who was blinded to data collection and patient diagnosis, listened and labeled the lung sound of coarse crackles, fine crackles, wheezing, stridor, squawk, normal breath sounds and decreased breath sounds from the seismometer patch once the data was rescaled, which was used as the standard labeling procedure. A total of 1939 wheezing sounds, 819 crackle sounds, and 2806 normal breath sounds four second segments were captured and utilized for the deep learning classifiers with the remaining lung sounds, such as stridor and squawk, not included in the dataset due to low number of datapoints. Out of those 96 patients, 40 of the patients had crackle sounds, 23 of the patients had wheezing sounds, 10 of the patients both adventitious lung sounds and 23 had normal breath sounds with details provided in Supplementary Table 6 and summarized in Supplementary Table 7. To record and display the data, the seismometer patch was connected to a data acquisition hub, similar to a Holter monitor.

Cough and snoring signal removal

Coughing and snoring are other symptoms of patients with respiratory diseases, such as obstructive sleep apnea, which were captured during data collection and led to more variance in the dataset[65]. To reduce variance in the seismometer patch dataset, coughing and snoring data was computationally removed from the dataset. The raw seismometer data is first parsed through a data cleaner to remove coughing and snoring data to ensure high quality data is used for computational WoB quantification and adventitious lung sound classification. Specifically, the data cleaner evaluated the spectral entropy of the 1d signal, removing tidal breathing instances exceeding 1.1 times the average spectral entropy amplitude than that of paradoxical breathing and removing deep breathing instances 1.1 times larger of the average spectral entropy amplitude than that of stridor, a known loud adventitious lung sound[66]. Spectral entropy was computed in MATLAB using Shannon entropy on the signal's normalized power spectral density in the frequency domain.

Signal denoising and analysis

With the seismometer patch, the out-of-plane PIVs were captured, cleaned, and then processed in MATLAB as shown in Fig. 1d. For WoB quantitative measurement, respiration rate was estimated using a moving average smoothing filter of the 10,000 nearest samples (0.5 s) on the 1D array, effectively capturing the prominent peaks of each breath cycle. The respiratory effort was quantified by the high-frequency MMG signal, which is a bandpass filtered data of the tidal breathing raw seismometer data from 80 to 200 Hz, to remove majority of heart sounds and possible wheezing PIVs with a filter order of 10. A summary of the WoB data processing pipeline is shown in Fig. 1d.

For the lung sound detection, the out-of-plane PIVs were filtered with a band pass filter of 60 Hz to 2000 Hz, corresponding to the main lung sound frequencies and to also remove the majority of heart sounds and motion artifact from the signal, with a filter order of 10[67]. The PIVs were then smoothened with a moving average filter with a window width of nine samples, similarly, used in digital stethoscope signal smoothening[68]. The data was then segmented into four second segments with 50% overlap and scaled from -1 to 1 for audible sound playback. Seismometer patch, acting as a contact microphone, were then played to an experienced physician to determine whether the audio contained crackles, wheezing or normal breath sounds. Since respiratory sounds have a wide range of frequencies[55,69], the seismometer patch PIVs recordings were analyzed via mel spectrograms, as shown in Figs. 3b and 4[69]. To create mel spectrograms, spectrograms from the PIVs were first created via Fast Fourier Transform (FFT) with a Hann window length of 1024 samples (approximately 50 ms) with a 50% overlap and the shown frequency range was set from 60 to 1200 Hz with 64 bands, creating an array of 340×64. The spectrogram frequency axis, y-axis, was then converted into in mel scale (m), a logarithmic scale correlated to how humans perceive pitch/frequency (f) as shown in Eq. (1), to create mel spectrograms:

$$m = 2595\log_{10}(1 + \frac{f}{700}) \tag{1}$$

To extract the chest wall movements for respiration rate and phase estimation from the seismometer data for the data fusion model, a moving average of the 10,000 nearest samples (0.5 s) on the raw seismometer data was applied to show when these adventitious lung sounds occur based on respiration phase. The upward ramps of amplitude plots indicate inspiration, while the downward ramps indicate expiration.

Work of breathing statistical quantification

WoB assessment composes of respiratory effort and respiration rate of accessory muscle groups. To quantify respiratory effort of each accessory muscle group, each accessory muscle group's high-frequency IPS MMG signal was divided by the estimated number of respiration cycles to estimate the average high-frequency IPS MMG of each respiration cycle, which was compared with the physician's visual classification of respiratory effort. Using the labels provided by experienced physician, a Mann Whitney U test was used to determine the statistical significance of patients with either normal or increased respiratory effort for each accessory group average high-frequency IPS MMG signal. A box-and-whisker plot was used to visualize the distribution of the average IPS high-frequency IPS MMG signal for all of the patients with normal and increased respiratory effort for each accessory muscle group. To estimate respiration rate, the average time difference between each peak and its consequent peak were used to estimate the number of respiration cycles in thirty seconds, which was then compared with physician's counting of number of respiration cycles. All WoB processing as shown in Fig. 1d was done in MATLAB.

Deep learning architecture: early data fusion convolutional neural network (CNN)

Since respiratory sounds are often correlated with respiratory phase, a data fusion deep learning architecture was proposed with inputs of PIVs mel spectrograms combined with its corresponding respiratory phase, enabling early data fusion, as shown in Fig. 3c. The data fusion was done by concatenating the normalized respiratory phase to the bottom of the mel spectrogram, resulting in a 340×65 array with data only from the seismometer patch. A 2D convolutional neural network (CNN) architecture was chosen for its strong performance in image detection and its capability for early data fusion. A total of 1939 wheezing sounds, 819 crackle sounds and 2806 normal breath sounds were used with no padding. Initially, a test set of 16 patients was separated, ensuring an unbiased evaluation. The training data was then separated into a Leave 16 Subject Out Cross Validation (L16SOCV), representing five folds, for hyperparameter optimization and was trained using TensorFlow GPU and Keras with a Nvidia GeForce GTX 1080 Ti GPU. Early stopping was utilized to monitor validation loss. No data augmentation was done. This architecture utilized five convolutional layers with filters of 128, 256, 256, 256 and 256 with a kernel size of (3,3). Each of the layer was followed with a dropout of 0.25 and a max pooling 2D step with a filter size of (2,2) and Rectified Linear Unit (ReLU) activation. After all the convolutional layers, a global average pooling 2D layer was applied to reduce spatial dimensionality. Following, a dense linear layer of 512 with ReLU activation was applied with a dropout of 0.5. Afterwards, a dense layer of 64 with ReLU activation was followed. Finally, a dense output was created. The variables were optimized by the Adam optimization algorithm with a learning rate of 5e-5 to reduce the custom loss function, designed to penalize the false negatives of crackles three times more than normal breath sounds to correct the dataset imbalance of lower number of crackles. The mini-batch size was set to four. The model was then evaluated on the 16 subjects test set, blind to training, as a classifier trained and tested on all lung locations.

To evaluate the 2D CNN model's efficacy on the test set, the deep learning architecture performance with solely mel spectrograms as the input was trained and tested, to determine the effects of early data fusion for classification. Furthermore, ResNet-18 architecture with inputs comprising of either early data fusion or only mel spectrograms were examined. Accuracy, sensitivity, specificity, precision, F1 and the area under the curve (AUC) of the Precision Recall (PR) were measured on all architectures to compare performances.

Results

Work of breathing (WoB) quantification

Traditionally, WoB is assessed qualitatively by physicians through visual evaluation of the patient's accessory respiratory muscle use, along with the breathing rate and pattern. To quantify both metrics, the seismometer patch, consisting of both out-of-plane and in-plane sensitivity, was positioned on/near each accessory muscle groups, shown in Fig. 1c. This setup measured muscle activation and respiration rate by capturing the outward and vertical movements of each accessory respiratory muscle group. To comfortably capture all accessory muscle movements, the seismometer patches were placed on the chest walls near each accessory muscle group as muscle movements propagate to surrounding skin. More specifically, to capture the scalene and sternocleidomastoid muscle activation, the seismometer patch was placed right below the clavicle region near the mid-clavicular region (Fig. 1c for location 1) as these muscles extend to the 1st and 2nd intercostal rib cage[70]. To quantify the intercostal muscle activation, the patch was placed near the 8th and 9th intercostal space in the anterior mid-clavicular region (location 2 in Fig. 1c) as past studies have found that the greatest change in muscle length for respiration is found in the anterior region of the body[64]. To capture abdominal muscle activation most consistently, the patch was placed above the umbilicus as shown in Fig. 1c for location 3. Each accessory muscle activation was quantified using the area under the curve of the 1D high-frequency MMG signal, a bandpass filtered signal in the frequency range of 80—200 Hz eliminating both heart sounds and possible adventitious lung sounds such as wheezing[57], as shown in Fig. 1d. Additionally, while previous studies have reported wheezing within 100–200 Hz[65], all wheezing sounds in this dataset were above 200 Hz. Respiration rate and pattern data were derived from smoothened (filtered) very low-frequency seismometer data. Both high-frequency MMG and respiration rate were then correlated with experienced physician's visual assessment of respiratory activity and respiration rate.

The seismometer patch placed on these locations can capture a patient's chest wall movements revealing the patient's breathing rate and pattern (normal or increased WoB). For instance, in patient 11 (Fig. 2a), the smoothened OPS and IPS data was analyzed where the OPS showed 3 distinct peaks whereas the IPS data accurately showed 15 respiratory cycles, denoted by the red stars, which matched the physician's bedside count. Because of the high respiration rate of an extrapolated rate exceeding 20 breaths/min, the patient is considered to have a high WoB. In another case, patient 17 exhibited paradoxical breathing, a sign of high work of breathing (WoB) and significant respiratory distress from the abdominal region, according to the physician's visual assessment. By extracting and smoothing OPS data with a moving average filter, we interestingly observed large, sudden peaks corresponding to muscle contractions, indicating paradoxical breathing, as shown in Fig. 2b, and matching with physician's clinical observation. Patient 17's corresponding IPS data showed a respiration rate of nine breaths in 30 s (matching to physician's count), extrapolating to less than 20 breaths per minute. As shown in Fig. 2c, the high-frequency MMG signal from in-plane movement revealed significant amplitude and variance, indicating increased vertical muscle movement. Despite the below 20 breaths per minute respiration rate, the presence of large sudden peaks due to paradoxical breathing and increased muscle activation from the abdominal region indicate that this patient has a very high WoB. Both out-of-plane and in-plane muscle movements captured by the seismometer patch provide key information regarding respiratory muscle activity, with in-plane data providing a more accurate representation of respiration rate.

The high-frequency IPS MMG analysis was conducted and quantified for each patient's accessory muscle groups to estimate the average muscle activation per respiratory cycle, with examples of varying respiratory effort in varying BMI patients shown in Supplementary Fig. 2 and correlated it with physician assessments of increased or normal respiratory effort. Examples include patients with high respiratory effort, high BMI patients with high respiratory effort and patients with normal respiratory effort from a wide range of BMI for each accessory muscle group. To show the distribution of increased and normal respiratory effort for each accessory

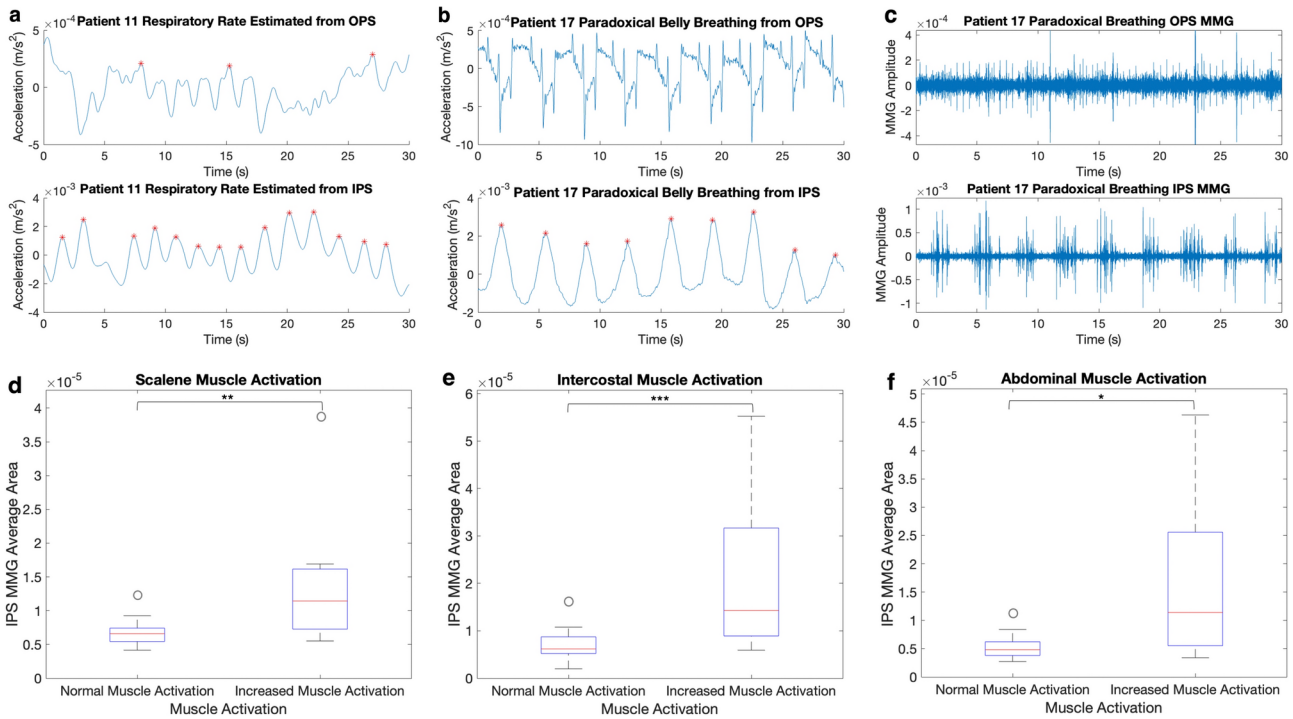

Fig. 2. Respiration rate and respiratory effort measurement captured by the seismometer patch containing both OPS and IPS chips placed on patients. (**a**) Respiration rate estimation shown for patient 11 where major peaks denoted by red stars representing each respiration cycle. In-plane measurement shows an accurate estimation for respiration rate. (**b**) Paradoxical breathing from patient 17 shown when seismometer patch placed on abdominal region where OPS low-frequency data shows sudden changes in the cycle correlating to paradoxical breathing while IPS can accurately estimate respiration rate indicated by the red star at each peak and matched with physician's visual count. (**c**) OPS and IPS high-frequency MMG signal from patient 17 on abdominal region derived from applying a bandpass filter, where the area under the curves is divided by the number of respiration cycles to calculate average high-frequency MMG signal. IPS high-frequency MMG is shown to be a more distinct indicator of respiratory effort. (**d**) Average in-plane high-frequency MMG signal for scalene muscle separated by physician assessment of normal and increased respiratory effort with statistical significance of < 0.01. (**e**) Average in-plane high-frequency MMG signal for intercostal muscle separated by physician assessment of normal and increased respiratory effort with statistical significance of < 0.001. (**f**) Average in-plane high-frequency MMG signal for scalene muscle separated by physician assessment of normal and increased abdominal effort with statistical significance of < 0.05.

respiratory group, the average high-frequency IPS MMG per respiration cycle of each patient is shown in a box and whisker plot for scalene, intercostal and abdominal muscles in Fig. 2d–f, respectively; each data point represents an individual patient. The Mann Whitney U Test was conducted and revealed statistical significance differences in muscle activation between normal and increased respiratory effort in the scalene ($p < 0.01^{**}$), intercostal ($p < .0.001^{***}$) and abdominal muscles ($p < 0.05$), as labeled by the physician's observation. Increased muscle activation was found in nine patients for the scalene, eight for intercostal, and seven for the abdominal muscles. These findings indicate that the average high-frequency IPS MMG correlates with muscle activation and respiratory effort for each accessory muscle group. Thus, combining a patient's average high-frequency IPS MMG and respiration pattern can therefore quantify non-invasively their WoB as a patient with either high average high-frequency IPS MMG or a respiratory rate of 20 breaths/minute can potentially be used as a signal for high WoB. This framework with the seismometer patch has the potential for adding another important clinical feature to longitudinal respiratory monitoring via the seismometer patch.

Early data fusion deep learning performance

Deep learning is widely used for automatic lung sound detection[69,71,72]. An early data fusion deep learning model was developed using mel spectrograms and corresponding respiration phase captured by the seismometer as inputs. Mel spectrograms visually represented the PIVs, the filtered output of the seismometer patch during deep breathing, with time (s) on the x-axis, frequency (Hz) in the mel scale on the y-axis and power in decibels (dB) as the color scale[69]. To extract respiration phase, the raw seismometer data was smoothened to estimate chest wall movement. An experienced physician labeled PIVs sound segments based on audio playback, as shown in the data processing flow chart in Fig. 3b with an example of sensor placement in Fig. 3c. These inputs were then concatenated and fed into the early data fusion 2D CNN architecture as shown in Fig. 3d. Due to the wide variety of patient data collected and the robustness of the sensor, no data augmentation was necessary. The dataset was initially partitioned with a dedicated test set of 16 patients blind to the model to determine the predictive model generalizability in real-world scenarios for an unbiased evaluation. A five-fold cross-validation approach, with 16 patients per fold, was utilized on the training dataset to mitigate overfitting and optimize hyperparameters. The 2D CNN early data fusion model utilized convolutional layers to extract features from the mel spectrogram. The layer's filter size increased initially and then remained constant, using a (3,3) kernel size to capture lung sound frequency variations across the 64-band mel spectrogram and respiration phase information from the bottom concatenated layer. Dropout and max pooling were integrated with convolutional layers to enhance generalization performance and mitigate overfitting. Additionally, ReLU activation functions were used to introduce non-linearity, aiding the model in learning the variations in crackle and wheezing frequencies. Employing a mini-batch size of four facilitated gradual learning of spatial representations. In addition, using a custom loss function also allowed for the model to decrease number of crackle false negatives, thus reduced the impact of data imbalance for the deep learning model. The performance of the data fusion deep learning architecture on the test set of four second seismometer data on determining if the recording is either a normal breath sound, crackle or a wheeze had great performance with an accuracy, sensitivity, specificity, precision and F1 score of 93.21%, 92.87%, 96.67%, 93.3% and 93.05%, showing its ability for generalizability in real-world scenarios. The AUC of the PR on the test set is 0.9736, which shows how well it can distinguish between categories. The confusion matrix of the deep learning architecture on the test set showed high sensitivity for each category, as shown in Fig. 3e, especially for crackles as they tend to be harder to detect with a stethoscope for less experienced professionals[51,52].

Comparing deep learning architectures performance

The performance of the custom 2D CNN deep learning architecture was also evaluated by comparing other deep learning architectures, such as testing the architecture with exclusively mel spectrograms as inputs to determine the influence of early data fusion on the deep learning performance. Additionally, a ResNet-18 architecture, adjusted to accommodate the input array size variations, was trained and evaluated with inputs of either early data fusion or only mel spectrograms. ResNet-18 was selected due to its well-established success and optimal layer depth for the specific task of classifying adventitious lung sounds[69].

As shown in Table 1, early data fusion inputs outperformed mel spectrogram inputs for both the custom 2D CNN and ResNet-18 architecture. The custom 2D CNN architecture has also outperformed ResNet-18 with both types of inputs with all architecture metrics. The highest performing model is the early data fusion with 2D CNN as it uses both mel spectrograms and respiration phase as data inputs. Similar results are also shown in the visual representations of the test set embeddings with corresponding silhouette score as shown in Supplementary Fig. 3 and Supplementary Table 8.

Lung acoustic map

Since the seismometer patch was placed on each conventional auscultation location (Fig. 3a), the data can be interpreted anatomically and physiologically to produce a comprehensive acoustic map of a patient's lungs, offering a novel, non-invasive and rapid, lung assessment that could complement traditional radiographic testing (chest x-ray or chest CT). As shown on the right of Fig. 4, the patient (patient 94) was found to have inspiratory coarse crackles, characterized by pronounced thick vertical yellow lines in the mel spectrogram with frequency range up to 400 Hz, similar to other coarse crackles[41]. The coarse crackles were identified in the basal regions of both the left and right posterior lung lobes (locations 8 and 9, denoted by the letter C). The patient also exhibited inspiratory fine crackles, shown by the temporally and spatially dense yellow area in the mel spectrogram with frequency range up to 300 Hz, similar to other fine crackles[41], in the right posterior lower and upper lobe along with the right anterior middle lobe (locations 3, 4 and 6, denoted by the letter C).

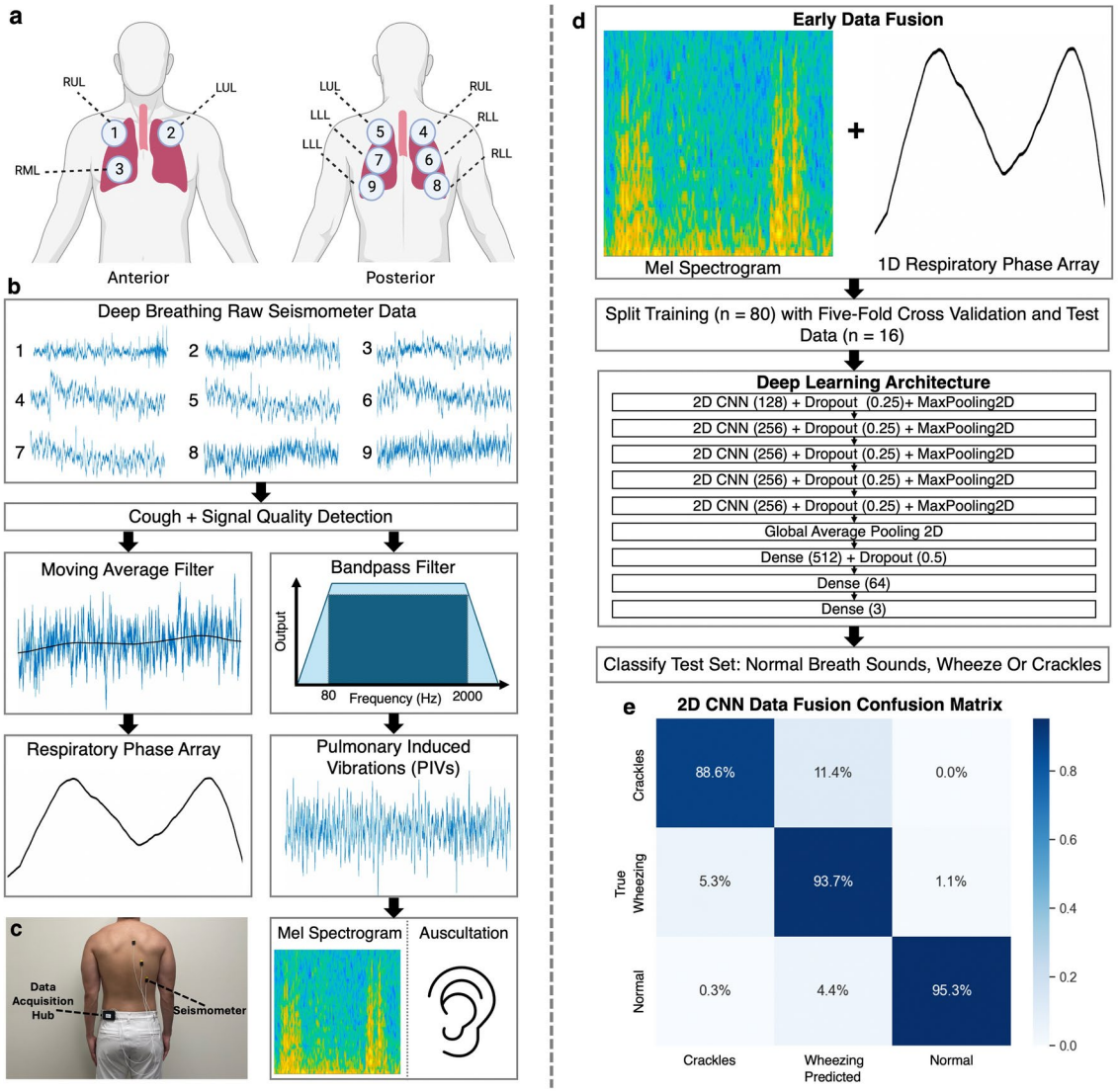

Fig. 3. Early data fusion deep learning data pipeline. (**a**) The seismometer patch was placed on each of the nine auscultation sites used in common comprehensive lung examination, which include the anterior and posterior of the chest. The site labels use a three-letter code: R represents right, M represents middle, L if the 1st letter represents left, if the 2nd represents lower and if the last letter represents lobe. (**b**) Deep breathing out-of-plane seismometer data from all auscultation sites were measured and segmented into four seconds with 50% overlap. The data then underwent through a cough and signal quality detection to remove coughing sounds. The cleaned data was filtered with a moving average to a capture 1D respiration phase array. The cleaned data is also bandpass filtered from 80 to 2000 Hz to isolate the pulmonary-induced vibrations (PIVs). PIVs were then converted into a mel spectrogram and made audible through rescaling from -1 to 1 to physicians to label normal breath sound, wheezing or crackles. (**c**) Example of seismometer patches taped on the posterior right lung auscultation zones. (**d**) For the deep learning model, PIVs patch mel spectrograms were concatenated with the 1D respiration phase array, a form of early data fusion, as inputs to the deep learning model. The data fusion data is then separated with 80 patients used for training via a five-fold cross validation (16 patients per each fold) with 16 patients as a test set, blind to the training. The deep learning architecture is then trained with a custom loss function and Adam optimizer. The model is then evaluated on the test set to provide real world generalizability of the model. (**e**) Confusion matrix of 2D CNN Data Fusion deep learning architecture on the test set with the predicted labels compared to the true labels showing high accuraccy for each category.

The correlation between lung acoustics and radiographic imaging is well-established, as the presence of crackles can signify either interstitial or alveolar infiltration (of either fluid, inflammation or infection) or interstitial fibrosis as shown in the imaging findings as curvilinear opacities (curved or wavy white lines) in the CT images on the left of Fig. 4. For this patient, the medical imaging examination was conducted one day prior to the seismometer data collection. The radiographic note of the CT scan image of Fig. 4 revealed mild pulmonary interstitial edema in the lung, shown with the white haziness in the lower lung region, correlating

Architecture	Accuracy	Sensitivity	Specificity	Precision	F1	AUC of PR
ResNet-18	0.8450	0.8439	0.9269	0.8506	0.8482	0.8918
ResNet-18 data fusion	0.8722	0.8688	0.9385	0.8757	0.8715	0.9293
2D CNN	0.9209	0.9183	0.9595	0.9184	0.9174	0.9684
2D CNN data fusion	0.9321	0.9287	0.9667	0.9330	0.9305	0.9736

Table 1. Comparisons of deep learning classifiers evaluated on test data (16 patients) from seismometer patch PIVs.

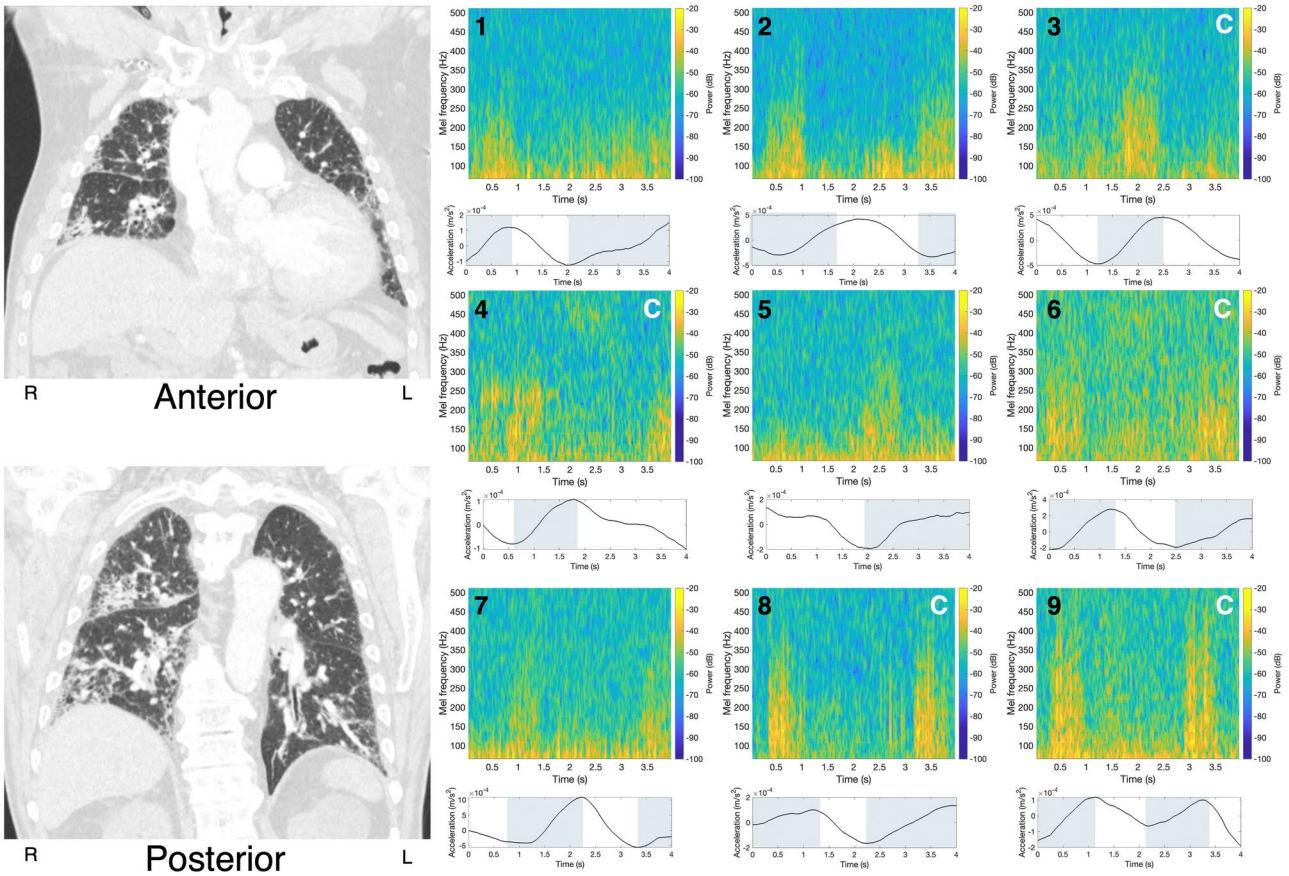

Fig. 4. CT image correlated to acoustic map captured by seismometer patch. CT image of anterior and posterior of the lung matching with PIVs of a pneumonia patient creating an acoustic map captured by seismometer patch. Crackles captured by the seismometer patch corresponded with CT image findings, such as increased interstitial and alveolar markings in the lungs. Each numbered location corresponds to the lung auscultation location in Fig. 3a. Respiration phase and amplitude in terms of acceleration of each auscultation location was captured by the seismometer patch with the grey box representing inspiration.

with the coarse crackles in the posterior basal regions of the lung (location 8 and 9)[60]. Additionally, as confirmed by radiographic notes, the imaging revealed more right than left diffuse reticulations and honeycombing in the lungs (indicating interstitial and alveolar fibrosis), as shown with the white network of fine lines and small thick-walled cysts (white holes), correlating with the fine crackles captured by the seismometer patch from the right posterior lower and upper lobe along with the right anterior middle lobe (location 3, 4 and 6)[61,62]. Similar findings have also been shown in X-ray images as well as shown in Supplementary Fig. 4. This patient was diagnosed with Usual Interstitial Pneumonia (UIP), an interstitial lung disease, which corresponded well to the seismometer patch data captured from the patient's lung auscultation locations. The physician, who was blinded to the patient's diagnosis, confirmed the audio signals of normal breath sounds, coarse crackles and fine crackles from the seismometer via sound playback and thus its utility in creating an acoustic lung map that can be used to lead to a patient's specific clinical diagnosis.

Discussion

Early detection of pathological respiratory signs can provide physicians critical information to assist in the diagnosis and monitoring of respiratory diseases in early stages of development and provide a needed novel means for disease screening and longitudinal respiratory monitoring[73]. Current assessments of physical signs of WoB and lung auscultation are subjective, lack inter-rater reliability and are not quantitative[26]. These methods are also inadequate for continuous monitoring and not scalable since they require a physician's presence. Therefore, a digital health lightweight device capable of detecting signs of respiratory diseases and respiratory distress are critical, as patients who are given timely treatment or have undergone needed intubation have a lower mortality rate[19,31]. To address this, we have used a wideband seismometer patch to detect increased WoB and adventitious lung sounds. The seismometer patch can distinctly capture increased respiratory effort via high-frequency MMG signals from all respiratory accessory muscle groups along with respiration rate and abnormal respiration pattern[43], notably paradoxical breathing, during tidal breathing. Moreover, high-frequency MMG has advantages over EMG, as a wideband seismometer can simultaneously capture both high-frequency MMG and low-frequency respiration patterns/rates, while EMG electrodes cannot capture respiration patterns/rates. The lightweight seismometer patch was also shown to effectively capture PIVs, such as faint crackles, from a patient's deep breaths. The seismometer patch can be extended with multiple heads to capture PIVs from multiple locations, creating a lung acoustic map that could enhance a physician's ability to diagnose and monitor respiratory conditions. With the seismometer, we created a framework to quantify WoB via statistically quantified respiratory effort via high-frequency MMG and respiration rate via low-frequency peak detection. The WoB quantification is first of its kind and correlated with the clinician bedside observation, a reliable sign of respiratory distress and failure[31]. The framework also includes a novel, robust deep learning architecture to detect adventitious lung sounds based off a diverse, real-world patient dataset. Additionally, this novel deep learning architecture utilizes an early data fusion approach, optimizing the detection of adventitious lung sounds, as respiratory sounds are correlated with the respiration cycle (Supplementary Table 1), both captured by the seismometer, which outperforms other deep learning architectures that utilizes only the lung sound as an input[74].

To enhance the framework for accurately representing a patient's WoB and lung sounds, additional data and standardized labeling by a panel of experienced physicians will provide a more systemized system. Currently, labeling tasks rely on a single physician, which could subjectivity and potential limitations. Thus, incorporating a physician panel for WoB and lung sound labeling, where two physicians provide labels and a third act acts a tiebreaker, would improve ground truth accuracy. In addition, using multiple labeling categories respiratory effort, such as normal, slightly increased and increased respiratory effort, may improve measurement precision[75,76].

Conclusion

In summary, we demonstrated that the robust and lightweight seismometer patch captured abnormal respiratory effort signatures from out-of-plane and in-plane muscle movement, acoustic signatures and respiration pattern from multiple critical respiratory locations simultaneously. When combined with WoB quantification and a robust deep learning algorithm, this framework has the potential to be utilized and deployed as a versatile respiratory monitoring system. This quick, non-invasive, quantitative, and accessible framework has the potential to reduce morbidity and mortality by enabling detection of worsening respiratory distress and diseases. Its ability to correlate with radiographic instruments through its anatomically generated acoustic lung map supports its use as a non-invasive longitudinal patient monitoring system by providing physicians more comprehensive information, such as sub-clinical respiratory changes. This technology opens the possibility for continuous respiratory monitoring and early detection, thereby offering physicians timely and precise data to enhance patient care for both acute and chronic respiratory diseases. Future studies for WoB quantification involve asking patients to be in various postures, such as lying down and sitting upright, to evaluate the impact of posture on WoB quantification as respiratory mechanics can vary in different positions[74].

Data availability

The datasets used and/or analyzed during the current study available from the corresponding author on reasonable request.

Code availability

The code will be available to any investigator upon request.

Received: 20 October 2024; Accepted: 4 March 2025
Published online: 15 March 2025

References

1. Bousquet, J., Khaltaev, N. G., Cruz, A. A. & World Health Organization. *Global Surveillance, Prevention and Control of Chronic Respiratory Diseases : A Comprehensive Approach*.
2. Dwyer-Lindgren, L. et al. Trends and patterns of differences in chronic respiratory disease mortality among US counties, 1980–2014. *JAMA J. Am. Med. Assoc.* **318**, 1136–1149 (2017).
3. Ruuskanen, O., Lahti, E., Jennings, L. C. & Murdoch, D. R. Viral pneumonia. *Lancet* **377**, 1264–1275 (2011).
4. Agustí, A., Vogelmeier, C. & Faner, R. COPD 2020: Changes and challenges. *Am. J. Physiol. Lung Cell Mol. Physiol.* **319**, L879–L883. https://doi.org/10.1152/AJPLUNG.00429.2020 (2020).
5. Confalonieri, M. et al. Acute respiratory failure in patients with severe community-acquired pneumonia a prospective randomized evaluation of noninvasive ventilation. *Am. J. Respir. Crit. Care Med.* **160**, 1585–1591 (1999).

6. Calverley, P. M. A. Respiratory failure in chronic obstructive pulmonary disease. *Eur. Respir. J.* **22**, 26s–30s (2003).
7. Quaderi, S. A. & Hurst, J. R. The unmet global burden of COPD. *Glob. Health Epidemiol. Genomics* https://doi.org/10.1017/gheg.2018.1 (2018).
8. COPD Trends Brief: Burden. *American Lung Association*.
9. Agustí, A., Vogelmeier, C. & Faner, R. COPD 2020: Changes and challenges. *Am. J. Physiol. Lung Cell. Mol. Physiol.* **319**, L879–L883. https://doi.org/10.1152/AJPLUNG.00429.2020 (2020).
10. Wunsch, H. et al. The epidemiology of mechanical ventilation use in the United States. *Crit. Care Med.* **38**, 1947–1953 (2010).
11. Vandevoorde, J. et al. Early detection of COPD: A case finding study in general practice. *Respir. Med.* **101**, 525–530 (2007).
12. Sekine, Y., Katsura, H., Koh, E., Hiroshima, K. & Fujisawa, T. Early detection of COPD is important for lung cancer surveillance. *Eur. Respir. J.* **39**, 1230–1240. https://doi.org/10.1183/09031936.00126011 (2012).
13. Bedoya, A. D. et al. Unanticipated respiratory compromise and unplanned intubations on general medical and surgical floors. *Respir. Care* **65**, 1233–1240 (2020).
14. Alqahtani, J. S. et al. Risk factors for all-cause hospital readmission following exacerbation of COPD: A systematic review and meta-analysis. *Eur. Respir. Rev.* **29**, 1–16. https://doi.org/10.1183/16000617.0166-2019 (2020).
15. Gattarello, S. et al. Decrease in Mortality in severe community-acquired pneumococcal pneumonia: Impact of improving antibiotic strategies (2000–2013). *Chest* **146**, 22–31 (2014).
16. Houck, P. M., Bratzler, D. W., Nsa, W., Ma, A. & Bartlett, J. G. Timing of antibiotic administration and outcomes for medicare patients hospitalized with community-acquired pneumonia. *Arch. Intern. Med.* **164**, 637–644 (2004).
17. Warusevitane, A., Karunatilake, D., Sim, J., Smith, C. & Roffe, C. Early diagnosis of pneumonia in severe stroke: clinical features and the diagnostic role of C-Reactive protein. *PLoS ONE* **11**, (2016).
18. Boniatti, M. M. et al. Delayed medical emergency team calls and associated outcomes. *Crit. Care Med.* **42**, 26–30 (2014).
19. Cyphers, V. E. et al. *Labored Breathing Pattern: An Unmeasured Dimension of Respiratory Pathophysiology*. https://doi.org/10.1101/2024.01.27.24301872 (2024).
20. Vestbo, J. et al. Global strategy for the diagnosis, management, and prevention of chronic obstructive pulmonary disease GOLD executive summary. *Am. J. Respir. Crit. Care Med.* **187**, 347–365. https://doi.org/10.1164/rccm.201204-0596PP (2013).
21. Noah, B. et al. Impact of remote patient monitoring on clinical outcomes: an updated meta-analysis of randomized controlled trials. *Npj Digit. Med.* https://doi.org/10.1038/s41746-017-0002-4 (2018).
22. Chau, J. P. C. et al. A feasibility study to investigate the acceptability and potential effectiveness of a telecare service for older people with chronic obstructive pulmonary disease. *Int. J. Med. Inform.* **81**, 674–682 (2012).
23. Dieffenderfer, J. et al. Low-power wearable systems for continuous monitoring of environment and health for chronic respiratory disease. *IEEE J. Biomed. Health Inform.* **20**, 1251–1264 (2016).
24. Whitehead, D. & Conley, J. The next frontier of remote patient monitoring: Hospital at home. *J. Med. Internet Res.* **25**, e42335 (2023).
25. Ashe, W. B. et al. Analysis of respiratory kinematics: a method to characterize breaths from motion signals. *Physiol. Meas.* **43**, 015007 (2022).
26. Tulaimat, A. & Trick, W. E. DiapHRaGM: A mnemonic to describe the work of breathing in patients with respiratory failure. *PLoS ONE* **12**, e0179641 (2017).
27. Apigo, M., Schechtman, J., Dhliwayo, N., Al Tameemi, M. & Gazmuri, R. J. Development of a work of breathing scale and monitoring need of intubation in COVID-19 pneumonia. *Crit. Care* https://doi.org/10.1186/s13054-020-03176-y (2020).
28. Fie, J. F. & Helms, C. M. Respiratory rate predicts cardiopulmonary arrest for internal medicine in patients. *J. Gen. Intern. Med.* **8**, 354–360 (1993).
29. Cabello, B. & Mancebo, J. Work of breathing. *Intensive Care Med.* **32**, 1311–1314 (2006).
30. Bellani, G. & Pesenti, A. Assessing effort and work of breathing. *Curr. Opin. Crit. Care* **20**, 352–358. https://doi.org/10.1097/MCC.0000000000000089 (2014).
31. Tulaimat, A., Gueret, R. M., Wisniewski, M. F. & Samuel, J. Association between rating of respiratory distress and vital signs, severity of illness, intubation, and mortality in acutely 111 subjects. *Respir. Care* **59**, 1338–1344 (2014).
32. Tulaimat, A., Patel, A., Wisniewski, M. & Gueret, R. The validity and reliability of the clinical assessment of increased work of breathing in acutely ill patients. *J. Crit. Care* **34**, 111–115 (2016).
33. Courtney, R. The functions of breathing and its dysfunctions and their relationship to breathing therapy. *Int. J. Osteopathic Med.* **12**, 78–85 (2009).
34. Saraya, T., Shimoda, M., Hirata, A. & Takizawa, H. Paradoxical respiration: 'Seesaw' motion with massive pulmonary consolidation. *BMJ Case Rep.* https://doi.org/10.1136/bcr-2015-213449 (2016).
35. Jonkman, A. H. et al. Analysis and applications of respiratory surface EMG: report of a round table meeting. *Crit. Care* https://doi.org/10.1186/s13054-023-04779-x (2024).
36. Sarlabous, L. et al. Efficiency of mechanical activation of inspiratory muscles in COPD using sample entropy. *Eur. Respir. J.* **46**, 1808–1811. https://doi.org/10.1183/13993003.00434-2015 (2015).
37. Sarlabous, L. et al. Inspiratory muscle activation increases with COPD severity as confirmed by non-invasive mechanomyographic analysis. *PLoS ONE* **12**, e0177730 (2017).
38. Lozano-García, M. et al. Surface mechanomyography and electromyography provide non-invasive indices of inspiratory muscle force and activation in healthy subjects. *Sci. Rep.* https://doi.org/10.1038/s41598-018-35024-z (2018).
39. Beck, T. W. et al. Mechnomyographic amplitude and frequency responses during dynamic muscle actions: A comprehensive review. *BioMed. Eng. Online* https://doi.org/10.1186/1475-925X-4-67 (2005).
40. Sang, B. et al. Identification of S2 paradoxical splitting in aortic stenosis subjects via seismocardiogram signals from a wearable accelerometer contact microphone. *IEEE Sens. J.* https://doi.org/10.1109/JSEN.2023.3280407 (2023).
41. Sang, B., Wen, H., Junek, G., Di Francesco, L. & Ayazi, F. Detection of respiratory crackles and respiration phase using a wearable MEMS contact microphone. In *2023 IEEE 19th International Conference on Body Sensor Networks (BSN)* 1–4 (Institute of Electrical and Electronics Engineers https://doi.org/10.1109/bsn58485.2023.10331153 (IEEE, 2023).
42. Sang, B. et al. An accelerometer-based wearable patch for robust respiratory rate and wheeze detection using deep learning. *Biosensors* **14**, 118 (2024).
43. Gupta, P., Wen, H., Di Francesco, L. & Ayazi, F. Detection of pathological mechano-acoustic signatures using precision accelerometer contact microphones in patients with pulmonary disorders. *Sci. Rep.* https://doi.org/10.1038/s41598-021-92666-2 (2021).
44. Dellinger, R. P. et al. Regional distribution of acoustic-based lung vibration as a function of mechanical ventilation mode. *Crit. Care* https://doi.org/10.1186/cc5706 (2007).
45. Gupta, P., Wen, H., Daruwalla, A., Moghimi, M. & Ayazi, F. A hermetically-encapsulated unidirectional accelerometer contact microphone for wearable applications. *2019 IEEE Sens.* (2019).
46. Gupta, P. et al. Precision wearable accelerometer contact microphones for longitudinal monitoring of mechano-acoustic cardiopulmonary signals. *NPJ Digit. Med.* https://doi.org/10.1038/s41746-020-0225-7 (2020).
47. Sang, B. *et al.* Detection of normal and paradoxical splitting in second heart sound (S2) using a wearable accelerometer contact microphone. In *2022 IEEE Sensors* 1–4 (IEEE, 2022). https://doi.org/10.1109/SENSORS52175.2022.9967056.
48. Bohadana, A., Izbicki, G. & Kraman, S. S. Fundamentals of lung auscultation. *N. Engl. J. Med.* **370**, 744–751 (2014).
49. Nath, A. R. & Capel, L. H. Inspiratory crackles–early and late. *Thorax* **29**, 223–227 (1974).

50. Melbye, H., Aviles Solis, J. C., Jácome, C. & Pasterkamp, H. Inspiratory crackles-early and late-revisited: Identifying copd by crackle characteristics. *BMJ Open Respir. Res.* **8**, e000852 (2021).
51. Sarkar, M., Madabhavi, I., Niranjan, N. & Dogra, M. Auscultation of the respiratory system. *Ann. Thorac. Med.* **10**, 158–168. https://doi.org/10.4103/1817-1737.160831 (2015).
52. Arts, L., Lim, E. H. T., van de Ven, P. M., Heunks, L. & Tuinman, P. R. The diagnostic accuracy of lung auscultation in adult patients with acute pulmonary pathologies: a meta-analysis. *Sci. Rep.* **10**, (2020).
53. Gavriely, N., Shee, T. R., Cugell, D. W. & Grotberg, J. B. Flutter in flow-limited collapsible tubes: A mechanism for generation of wheezes. *J. Appl. Physiol.* **66** (1989).
54. Cruz, J. D. L. T. et al. Monophonic and polyphonic wheezing classification based on constrained low-rank non-negative matrix factorization. *Sensors* **21**, 1–23 (2021).
55. Meslier, N., Charbonneau, G. & Racineux, J. L. Wheezes. *Eur. Respir. J.* **8**, 1942–1948. https://doi.org/10.1183/09031936.95.08111942 (1995).
56. Pasterkamp, H., Kraman, S. S. & Wodicka, G. R. State of the art respiratory sounds advances beyond the stethoscope. *Am. J. Respir. Crit. Care Med.* **156**, 974–987 (1997).
57. Islam, M. A., Sundaraj, K., Ahmad, R. B. & Ahamed, N. U. Mechanomyogram for muscle function assessment: A review. *PLoS ONE* **8**, e58902 (2013).
58. De Troyer, A., Kirkwood, P. A. & Wilson, T. A. *Respiratory Action of the Intercostal Muscles*. https://doi.org/10.1152/physrev.00007.2004 (2005).
59. Dellweg, D., Haidl, P., Siemon, K., Appelhans, P. & Kohler, D. Impact of breathing pattern on work of breathing in healthy subjects and patients with COPD. *Respir. Physiol. Neurobiol.* **161**, 197–200 (2008).
60. Assaad, S., Kratzert, W. B., Shelley, B., Friedman, M. B. & Perrino, A. Assessment of pulmonary edema: Principles and practice. *J. Cardiothorac. Vasc. Anesth.* **32**, 901–914. https://doi.org/10.1053/j.jvca.2017.08.028 (2018).
61. Fukumitsu, T. et al. The acoustic characteristics of fine crackles predict honeycombing on high-resolution computed tomography. *BMC Pulm. Med.* https://doi.org/10.1186/s12890-019-0916-5 (2019).
62. Sgalla, G. et al. 'Velcro-type' crackles predict specific radiologic features of fibrotic interstitial lung disease. *BMC Pulm. Med.* https://doi.org/10.1186/s12890-018-0670-0 (2018).
63. Yoo, J. Y. et al. Wireless broadband acousto-mechanical sensing system for continuous physiological monitoring. *Nat. Med.* **29**, 3137–3148 (2023).
64. De Troyer, A., Kirkwood, P. A. & Wilson, T. A. Respiratory action of the intercostal muscles. *Physiol. Rev.* **85**, 717–756 (2005).
65. Piirila, P. & Sovijarvi, A. R. A. Objective assessment of cough. *Eur. Respir. J.* **8**, 1949–1956. https://doi.org/10.1183/09031936.95.08111949 (1995).
66. Pfleger, A. & Eber, E. Assessment and causes of stridor. *Paediatr. Respir. Rev.* **18**, 64–72. https://doi.org/10.1016/j.prrv.2015.10.003 (2016).
67. Homs-Corbera, A., Fiz, J. A., Morera, J. & Jané, R. Time-frequency detection and analysis of wheezes during forced exhalation. *IEEE Trans. Biomed. Eng.* **51**, 182–186 (2004).
68. Leng, S. et al. The electronic stethoscope. *BioMed. Eng Online* https://doi.org/10.1186/s12938-015-0056-y (2015).
69. Kim, Y. et al. Respiratory sound classification for crackles, wheezes, and rhonchi in the clinical field using deep learning. *Sci. Rep.* **11**, (2021).
70. Raper, A. J., Taliaferro Thompson, W., Shapiro, W. & Patterson, J. L. Scalene and sternomastoid muscle function. *Am. Physiol. Soc.* **21**, 497–502 (1966).
71. Kim, B. J., Kim, B. S., Mun, J. H., Lim, C. & Kim, K. H. An accurate deep learning model for wheezing in children using real world data. *Sci. Rep.* https://doi.org/10.1038/s41598-022-25953-1 (2022).
72. Hoon Lee, S. et al. Fully portable continuous real-time auscultation with a soft wearable stethoscope designed for automated disease diagnosis. *Sci. Adv.* https://doi.org/10.1126/sciadv.abo5867 (2022).
73. Wilkinson, T. M. A., Donaldson, G. C., Hurst, J. R., Seemungal, T. A. R. & Wedzicha, J. A. Early therapy improves outcomes of exacerbations of chronic obstructive pulmonary disease. *Am. J. Respir. Crit. Care Med.* **169**, 1298–1303 (2004).
74. Romei, M. et al. Effects of gender and posture on thoraco-abdominal kinematics during quiet breathing in healthy adults. *Respir. Physiol. Neurobiol.* **172**, 184–191 (2010).
75. McCollum, E. D. et al. Digital auscultation in PERCH: Associations with chest radiography and pneumonia mortality in children. *Pediatr. Pulmonol.* **55**, 3197–3208 (2020).
76. McCollum, E. D. et al. Listening panel agreement and characteristics of lung sounds digitally recorded from children aged 1–59 months enrolled in the pneumonia etiology research for child health (PERCH) case–control study. *BMJ Open Respir. Res.* **4**, (2017).

Acknowledgements

This work was supported by grants from the Georgia Research Alliance (GRA) and National Institutes of Health (NIH) R03 EB029099. The content is solely the responsibility of the authors and does not necessarily represent the official views of Georgia Institute of Technology, Emory University, and its affiliated academic health care centers.

Author contributions

Guarantor: F.A. takes responsibility for the integrity of the complete work and the final decision to submit the manuscript. Sensor Design: H.W., G.J., F.A. Study concept and design: B.S., L.D., F.A. Data Acquisition and Patient Study: B.S, W.N, L.D. Data Processing: B.S. Critical review and interpretation of data: All authors. Drafting of Manuscript: B.S. Critical revision of manuscript: All authors. Obtaining funding: F.A.

Declarations

Competing interests

Farrokh Ayazi is an inventor of the technology being studied and the purpose of this project is to explore its commercialization. The terms of arrangement have been reviewed and approved by Georgia Institute of Technology in accordance with its conflict-of-interest policies. All the remaining authors declare no conflict of interest.

Additional information

Supplementary Information The online version contains supplementary material available at https://doi.org/10.1038/s41598-025-93011-7.

Correspondence and requests for materials should be addressed to B.S.